International Journal of Design & Nature and Ecodynamics
Vol. 21, No. 10, October, 2026, pp. 2941-2955
Journal homepage: http://iieta.org/journals/ijdne

Fabrication of CTAB-Bentonite/ZnO Nanocomposite for Enhanced Adsorption of Synthetic Dyes from Aqueous Solutions

Nabaa Mahdi Ali, Intidhar Jabir Idan*

Department of Environmental Engineering, College of Engineering, University of Babylon, Babylon 51001, Iraq

Corresponding Author Email: eng.intidhar.jabir@uobabylon.edu.iq

Copyright: ©2026 The authors. This article is published by IIETA and is licensed under the CC BY 4.0 license (http://creativecommons.org/licenses/by/4.0/).

https://doi.org/10.18280/ijdne.211008

Received: 9 August 2026
Revised: 1 October 2026
Accepted: 12 October 2026
Available online: 31 October 2026

Keywords:
adsorption, CTAB, malachite green, nanocomposite, reactive red 152, ZnO-nano-bentonite

ABSTRACT

In this study, a new, highly efficient organic nanocomposite was synthesized to remove cationic and anionic textile dyes from single and binary solutions. Bentonite (BN) clay was initially chemically modified with cetyltrimethylammonium bromide (CTAB) to improve its surface properties. Subsequently, the modified bentonite was successfully converted into a nanocomposite using zinc oxide nanoparticles–CTAB-nano-BN. Fourier transform infrared spectroscopy (FTIR), scanning electron microscopy (SEM), and X-ray diffraction (XRD) were used to characterize the CTAB-nano-BN adsorbent. To evaluate the efficiency of the CTAB-nano-BN adsorbent, batch-mode adsorption experiments were used to remove malachite green (MG) and reactive red 152 (RR 152) dyes from single and binary systems under different operating conditions. In the binary system, CTAB-nano-BN exhibited maximum removal efficiency of 99.99% for MG dye under various operating conditions and 99.93% for RR 152 dye at 1 g dose, 100 mg/L, 60 min, and pH = 6. To understand the adsorption mechanism in the two systems, isotherm models were used. Furthermore, "first- and second-order pseudo-kinetic models" were employed to evaluate the reaction rates, where MG dye fit well with Jain and Snoeyink Modified Extended Langmuir (JSME), while RR 152 dye fit well with the Extended Freundlich (EF) model and both dyes were best described by the pseudo-second-order model. This study aims to highlight the potential of CTAB-nano-BN as a promising adsorbent for removing positive and negative dyes.

1. INTRODUCTION

Industries like textiles, paper, and cosmetics use large amounts of dyes, causing major environmental issues, particularly water pollution [1]. Dyes are difficult to break down in textile effluent because textile waste contains a wide range of chemicals and materials. This wastewater often contains large amounts of unfixed dyes [2]. Textile dyes are considered major water pollutants because they affect the physical and chemical properties of water. They impede the passage of light into water bodies, affecting photosynthesis and increasing biological and chemical oxygen demand. They also affect the growth and development of living organisms and are toxic and carcinogenic to humans, among other effects [3, 4]. In fact, textile wastewater contains a mixture of dyes with different properties. Therefore, the biggest challenge lies in treating textile wastewater containing multiple types of dyes, as few comprehensive studies have examined the interactions between different dye molecules and their effects on treatment processes [5]. Adsorption is the preferred process for removing dyes from aqueous solutions because it is simple to design and operate, highly effective, low-cost, and energy-efficient [6]. The sustainable development of natural adsorbents for environmental remediation is important, particularly because these materials reduce reliance on synthetic alternatives. Natural materials can be utilized—incorporating design strategies based on physical and chemical modification—to produce adsorbents capable of treating pollutants with diverse characteristics [7].

Adsorbents are an important factor in adsorption processes, and various adsorbents have been used, including clay materials such as zeolite, sepiolite, bentonite, kaolinite, and montmorillonite. These materials are widely used because of their diverse structural and surface properties, large surface area, chemical stability, high adsorption capacity, economic cost, non-toxicity, abundance, and high ion-exchange efficiency [8]. Bentonite is described as a smectite and phyllosilicate clay mineral. It has a permanent negative charge and usually occurs as sodium or calcium bentonite [9]. Using untreated bentonite in water treatment has drawbacks, including material selectivity, clay swelling, and settling issues [10]. Recently, researchers have explored nanotechnology for removing organic pollutants from wastewater. Nano-bentonite (Nano-BN) is one example, valued for its strong adsorption of various dyes and its large surface area [11]. ZnO is widely used in the treatment of wastewater because of its strong oxidizing properties. However, it has drawbacks such as instability in acidic conditions, photocorrosion, aggregation, and difficulty isolating it from the water-based phase, which limit its use. To

address these issues, combining ZnO with a suitable material can help. Permeable inorganic bentonite clay is a good option for this purpose [12]. According to Alshabanat et al. [13], combining ZnO NPs (chitosan-prepared nanoparticles) with bentonite clay enhances the adsorbent's effectiveness in removing pollutants from contaminated water. The resulting compound shows improved expansion and ion-exchange properties. Both bentonite and zinc oxide nanoparticles are abundant and inexpensive, making them suitable for treating and removing organic pollutants [14].

On the other hand, clay has a negative charge, which reduces the adsorption efficiency of anionic dyes. Therefore, it is necessary to improve the adsorption of negatively charged dyes by adding materials that enhance clay adsorption [9]. To overcome this obstacle and expand bentonite's application, researchers modified it with various organic materials, such as cetyltrimethylammonium bromide (CTAB). In this process, the cations between the clay layers are replaced by cations from the organic materials. This modification alters the surface charge and increases the affinity of the bentonite clay for adsorbing anionic dyes [15, 16]. CTAB is a cationic surfactant known for its strong, active surface, antibacterial effects, and stability across different pH values. When used to modify bentonite, it improves the clay's internal structure, boosts its electrical efficiency, and helps remove anionic dyes more effectively [17]. Moreover, once the modified bentonite clay is saturated with dyes, it can be disposed of at an authorized facility equipped to handle industrial waste, in accordance with the dye's chemical and environmental characteristics of the dye substance. This measure aims to prevent the release of adsorbed dyes into the environment and to minimize the environmental impact associated with unsafe disposal.

Bentonite clay is selected as an adsorbent material because its negatively charged, layered structure, abundant cation-exchange sites, and expandable interlayer spaces collectively provide a natural platform capable of engineering modification. Consequently, designing a bentonite-based adsorbent entails first identifying the pollutant-binding mechanism, then modifying its structure and surface to increase active sites and affinity for the target pollutants. The current scientific literature on a comprehensive, in-depth study addressing the sequential dual modification of bentonite using CTAB first, followed by its combination with zinc oxide nanoparticles, is scarce. Therefore, the aims of this study are to develop an adsorbent material based on bentonite clay to remove malachite green (MG) and reactive red 152 (RR 152) dyes from the single and binary systems under laboratory conditions. The material was characterized by several techniques and evaluated in a binary system for removal percentage, adsorption capacity, dosage, contact time, and pH.

2. MATERIAL AND METHODOLOGY

2.1 Material

Three main types of materials were used: raw bentonite, chemicals to produce CTAB-nano-BN, and dyes.

2.1.1 Raw calcium bentonite

We obtained non-activated bentonite clay powder from the Geological Survey of Iraq in Baghdad. Figure 1 displays the raw bentonite.

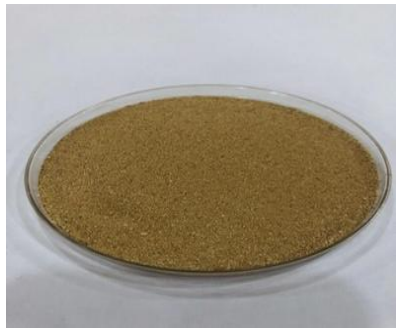

Figure 1. Raw calcium bentonite

2.1.2 Chemicals

Table 1 lists the chemicals used in this research, including their purity grade and applications. The properties of ZnO nanoparticles are particle size 10–30 nm, purity 99.8%, powder/nanopowder, white to light yellow, nanopowder/nanoparticles, CAS number 1314-13-2, and supplier SkySpring Nanomaterials. The properties of CTAB are CAS number 57-09-0, EC number 200-311-3, assay 99.00–101.00%, and supplier HIMEDIA.

2.1.3 Dyes

Malachite green (MG), a cationic solid surfactant dye, and RR, an anionic reactive dye, were used as adsorbates to assess CTAB-nano-BN adsorption capacity. Figure 2 shows the structures of MG and RR, and Table 2 lists their properties.

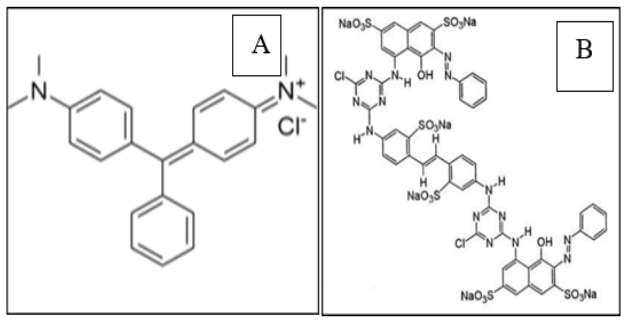

Figure 2. The chemical structure of (a) malachite green (MG) [18] and (b) reactive red 152 (RR 152) [19]

2.2 Methods

2.2.1 Preparation of adsorbate

To prepare a dye solution, dissolve 1 g of each dye in 1 L of distilled water to produce a solution of dyes with a concentration of 1000 mg/L.

Table 1. List of chemicals used in research

Material	Formula	Molecular Weight (g/mol)	Purity Grade (%)	Purpose
Cetyltrimethylammonium bromide	$C_{19}H_{42}BrN$	364.45	99	For surface charge modification
ZnO	ZnO	81.38	99.8	To prepare nano-BN
Sodium hydroxide	NaOH	40.00	98	For pH adjustment
Hydrochloric acid	HCl	36.46	99	For pH adjustment

Table 2. Chemical formula and properties of malachite green (MG) and reactive red 152 (RR 152)

Commercial Dye's Name	Name of C. I	λ_{max} (nm)	Molecular Weight (g/mol)	Chemical Formula
Basic Green 4	MG	618	927.02	C_{52} H_{54} N_4 O_{12}
Reactive Red 152	RR 152	554	1752.11	$C_{52}H_{30}Cl_2N_{14}Na_6O_{20}S_6$

For a binary system, mix the two dyes in a 1:1 ratio. In other words, 1 g of each dye was mixed with 500 mL of distilled water separately and thoroughly dissolved. The solution was left to stand to ensure complete dissolution. To prepare a binary solution, the two dye solutions were mixed: 500 mL of MG and 500 mL of RR, resulting in a total volume of 1000 mL.

For single and binary systems, each dye solution was diluted to a series of concentrations (5, 10, 15, 20, 25, and 30 mg/L) to plot the calibration curve. The absorbance is measured twice for each concentration in a dual-component system: once by fixing the wavelength of MG at λ_{max} = 618 nm and then by fixing the wavelength of the RR 152 dye at λ_{max} = 554 nm.

2.2.2 Preparation of organic nano-bentonite

Three steps were used to prepare the organic nano-BN adsorbent. The first step was to purify the bentonite clay sample. Bentonite was washed with water to remove dust and impurities until the rinse water ran clear, then washed again with deionized water. The sample was dried at 70 ℃ in an oven (MATEST A00711, Italy) until fully dry, then ground and sieved through 16- and 200-mesh sieves. The dried bentonite clay was passed through the 16-mesh sieve, then through the 200-mesh sieve. The clay remaining on the 200-mesh sieve was collected and stored in glass containers for later use.

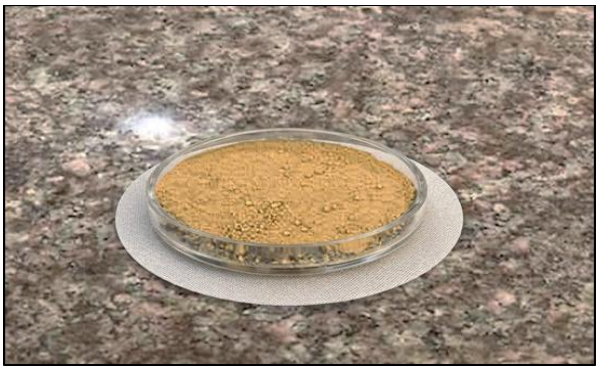

Figure 3. CTAB-nano-BN

The second step, organic calcium bentonite clay, was produced following the method previously described by Iqajtaoune et al. [20] using cationic surfactant (CTAB). 8 g of bentonite clay was dispersed in 250 mL of distilled water and stirred for 1 h in a shaker at 25 ± 2 ℃. Afterward, 0.5 g of CTAB was added, and the mixture was stirred for an additional 2 h; the weight percentage of each material was calculated (the mass ratio was 0.06 g CTAB per 1 g bentonite). The cationic exchange capacity of calcium bentonite, as reported by Naji and Ali [21], is 65 milliequivalents (meq)/100 g. For the 8 g of bentonite used, 0.5 g of CTAB represents 26.4% of the available cation exchange capacity. The resulting product was washed several times with distilled water to remove excess CTAB, then it was centrifuged at 4000 rpm for 10 minutes and dried in an oven at 70 ℃ until completely dry. The resulting clay was named CTAB-BN. The final step was to prepare CTAB-nano-BN, the nano-adsorbent, as described by Al-Saade et al. [22]. 10 g of CTAB-BN was added to 50 mL of distilled water, along with 0.05g of ZnO nanoparticles, and the mixture was stirred in a shaker at 200 rpm for 9 h. The CTAB-nano-BN was dried at 70 ℃ and sieved (clay remaining on sieve no. 200 was taken), then kept in a closed container prior to use. Figure 3 shows CTAB-nano-BN.

2.3 Adsorption experiments

Batch adsorption tests were utilized to investigate the adsorption of MG and RR 152 dyes from non-competitive and competitive solutions onto CTAB-nano-BN. For each test, we added 100 mL of the dye solution to a 250 mL Erlenmeyer flask. The effect of adsorbent dose (0.01, 0.2, 0.4, 0.6, 0.8, 1, 1.2, and 1.4 g), initial dye concentration (10, 20, 40, 60, 80, 100, 120, and 140 mg/L), contact time (15–180 minutes), and pH (2, 4, 6, 8, 10) value was studied. Each flask was sealed with aluminum foil to prevent leakage and evaporation. The flasks were shaken at 250 rpm at 25 ± 2 ℃ using a conventional stirrer (LAPTECH, Germany); all experiments were conducted three times (n = 3). After shaking, all samples were filtered using NICE Ashless fast filter paper prior to the analysis to minimize the interference of the CTAB-nano-BN with the absorbance analysis, and their absorbance was measured with a UV-1800 spectrometer (Japan) at λ_{max} 618 nm for MG and 554 nm for RR 152 without any dilution. After the single-adsorption experiment, we determined the amount of each dye in solution using a linear relationship between absorbance (A) and sample concentration (C), as described by Lambert's law and shown in Eq. (1) [23].

$$A = KC + E \tag{1}$$

where,

A: absorbance at wavelength λ,

K: absorbance coefficient (L/mg),

C: dye concentration (mg/L),

E: intercept of the relationship.

In a binary system, the two dyes' equilibrium concentrations are measured as in Eqs. (2) and (3) [24].

$$CG = \frac{(KR2 * A1) - (KR1 * A2)}{(KG1 * KR2) - (KG2 * KR1)} \tag{2}$$

$$CR = \frac{(KG1 * A2) - (KG2 * A1)}{(KG1 * KR2) - (KG2 * KR1)} \tag{3}$$

where, KG1 and KR1 are the calibration coefficients for MG and RR 152 dyes at $\lambda_{1,\,max}$. KG2 and KR2 at $\lambda_{2,\,max}$. A1 and A2 are the absorbance of both dyes at $\lambda_{1,\,max}$ and $\lambda_{2,\,max}$.

Therefore, to calculate the concentration of each dye in the binary solution, four calibration curves are constructed for each dye in the multi-component dye, two curves for each wavelength, to determine four calibration coefficients, as shown in Figure 4.

From Figure 4, four calibration curves were obtained, which are:

$y = 0.0889x$ with $R^2 = 0.996$ for MG dye and $y = 0.0122x$ with $R^2 = 1$ for RR 152 dye at $\lambda_{max} = 618$ nm

$y = 0.0131x$ with $R^2 = 0.997$ for MG dye and $y = 0.011x$ with $R^2 = 0.998$ for RR 152 dye at $\lambda_{max} = 554$ nm

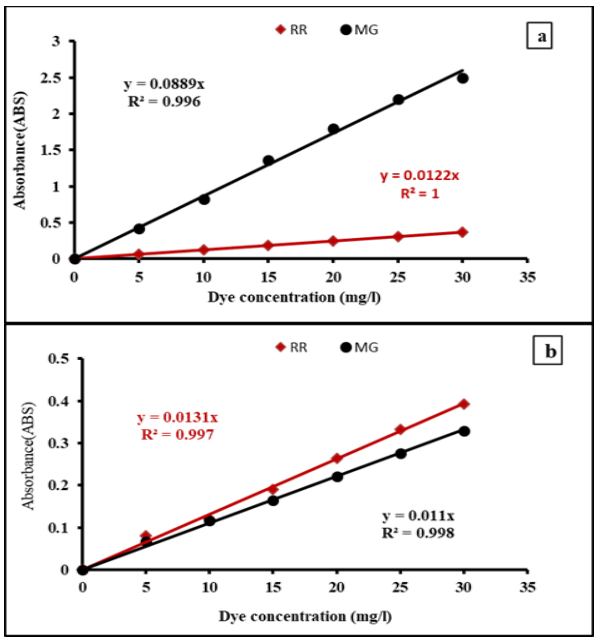

Figure 4. Calibration curve for malachite green (MG) and reactive red 152 (RR 152) dyes (a) at $\lambda_{1,\,max} = 618$ nm and (b) at $\lambda_{2,\,max} = 554$ nm

From the above equations, the calibration constants for MG and RR 152 are:

KG1 = 0.0889, KR1 = 0.0122 measured at $\lambda_{1,\,max} = 618$ nm

KG2 = 0.011, KR2 = 0.0131 measured at $\lambda_{1,\,max} = 554$ nm

As a result, the concentrations of MG and RR 152 dyes were calculated from Eqs. (4) and (5), respectively.

$$CG = \frac{(0.0131 * A1) - (0.0122 * A2)}{(0.0889 * 0.0131) - (0.011 * 0.0122)} \quad (4)$$

$$CR = \frac{(0.0889 * A2) - (0.011 * A1)}{(0.0889 * 0.0131) - (0.011 * 0.0122)} \quad (5)$$

The accuracy of the simultaneous determination of MG and RR 152 dyes was verified at a concentration of 20 mg/L each, yielding recovery rates of 100.7% for MG and 99.3% for RR. Quantification using the calibration equations was limited to residual concentrations following the adsorption process; all measured values fell within the established calibration range; therefore, no extrapolation beyond the calibration range was required.

The removal efficiency and amount of dye (mg) adsorbed per unit weight of adsorbent (g) can be calculated from Eqs. (6) and (7).

$$\text{Removal}, \% = \frac{c_i - c_e}{c_i} * 100\% \quad (6)$$

$$qe = \frac{c_i - c_e}{m} * v \quad (7)$$

where, C_i is the initial MG or RR 152 dye concentration, mg/L; C_e is the equilibrium concentration of MG and RR 152 dyes, mg/L; m is the mass of CTAB-nano-BN in grams; v refers to the volume of the binary solution in liters.

3. RESULT AND DISCUSSION

3.1 Characterization of CTAB-nano-BN

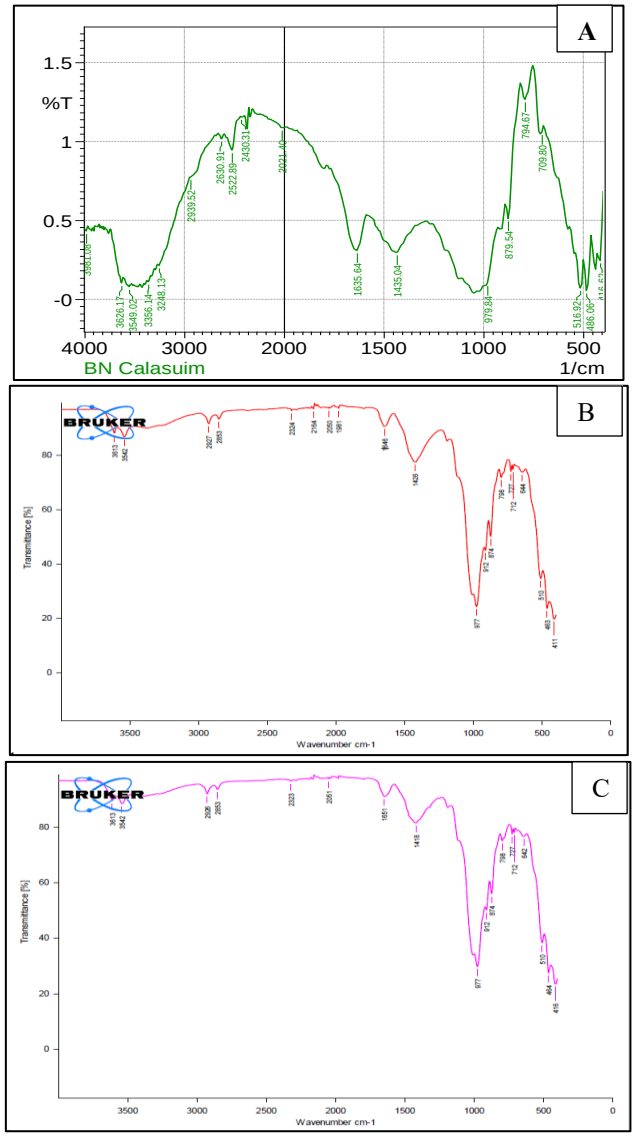

Figure 5. Fourier transform infrared spectroscopy (FTIR) analysis for (A) Nano-BN, (B) CTAB-nano-BN, and (C) CTAB-nano-BN after adsorption of two dyes from the binary system

3.1.1 Fourier transform infrared spectroscopy

Fourier transform infrared spectroscopy (FTIR) was used to determine the composition of raw and CTAB-nano-BN and to characterize the binding of dye molecules, as shown in Figure 5. The spectrum showed distinct absorption bands indicative of specific groups. As shown in Figure 5(A) for raw bentonite, the band at 3626.17 cm^{-1} can be attributed to the OH stretching vibration of Al^{3+} cations in the octahedral layer [25]. After modification, the peaks shifted to 3613 cm^{-1} [26]. Bending vibrations at 3549.02 cm^{-1}, 3356.14 cm^{-1}, 3248.13 cm^{-1}, and 1635 cm^{-1} correspond to the vibration of the OH bond, which

is attributed to the presence of water or moisture between the BN layers [25, 27]. After CTAB adjustment shown in Figure 5(B), the water content decreased, and peaks at 3542, 1426, and 1646 cm^{-1} were observed [28, 29]. Bending at 794 cm^{-1} shows bending vibrations (Si-O) which are associated with the presence of quartz and silica, while 516 bending vibrations are due to the presence of a bond (Al-O-Si) and represent the absorption peaks of the primary components of the bentonite clay, including SiO_2, Al_2O_3, Fe_2O_3, and MgO [30]. A similar result was reported in the vibration range of 709–794 cm^{-1} [31]. After improving bentonite, the Si-O and Si-O-Al bonds shifted to 798 cm^{-1} and 510 cm^{-1}, respectively [32, 33]. The new peaks at 2927 cm^{-1} and 2853 cm^{-1} refer to the vibrational range (C-H), and their presence indicates that the CTAB molecule is present, indicating successful modification [29, 34-36]. The vibrations at 712 and 644 cm^{-1} could be attributed to Zn-O through the formation of zinc nanoparticles [37]. CTAB-nano-BN after adsorption of two dyes as shown in Figure 5(C), some peaks including 2926, 2323, 2051, 1651,1418, 642, 464, and 416 cm^{-1} were shifted in to 2927, 2324, 2050, 1426, 1646, 644, 463, and 411 cm^{-1} this shift of the peaks is considered evidence of adhesion of the two dyes onto the surface of the material, which has been proven by the study [38].

3.1.2 Scanning electron microscopy

Scanning electron microscopy (SEM) is used to investigate the reaction products and the formation of raw and CTAB-nano-BN. SEM images in Figure 6(A) show that ordinary raw bentonite has a comparatively heterogeneous surface, with minor pores observed. Modifying bentonite with CTAB and attaching it to zinc oxide nanoparticles resulted in morphological changes in the bentonite structure, as shown in Figure 6(B). ZnO nanoparticles were observed to accumulate mainly on the bentonite surface rather than forming separate aggregates. The presence of CTAB caused the ZnO nanoparticles to assume different shapes, such as rectangles, cubes, and spheres. This is due to electrostatic attraction between the vertical surfactant groups and the zinc oxide nanoparticles, leading to greater ZnO accumulation on the bentonite surface and the formation of different shapes. This modification resulted in a final composite with a high surface area and a well-distributed nanoparticle structure, free of agglomeration [37, 39]. In Figure 6(C), the surface of the organic nano-BN appears as a single mass with no interfacial spaces present. The negatively charged nano-surface of the bentonite adsorbed the cationic dye, while the positively charged vertical groups adsorbed the anionic dye. Both dyes adsorbed more efficiently, forming a dense layer of dye particles.

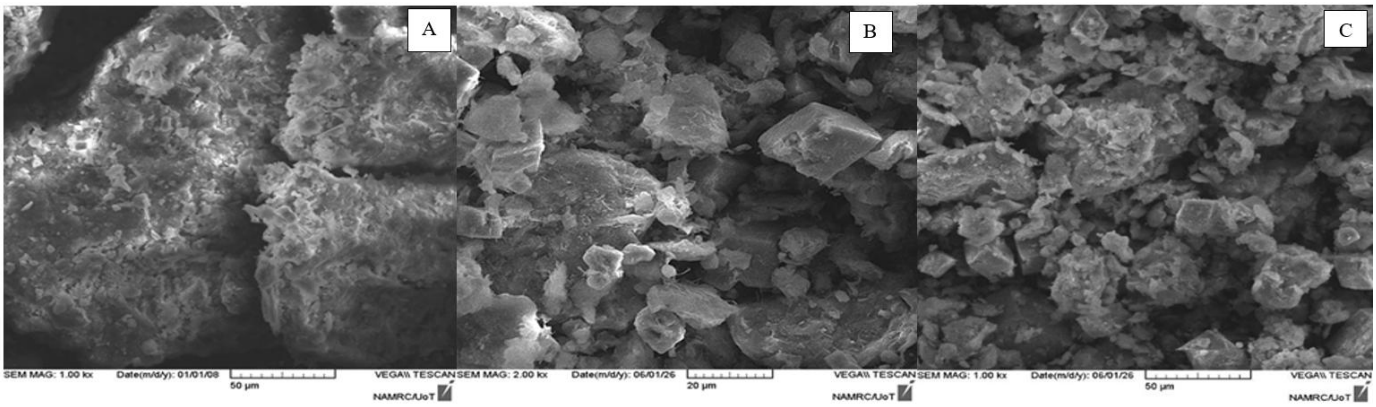

Figure 6. Scanning electron microscopy (SEM) analysis of (A) raw bentonite, (B) CTAB-nano-BN, and (C) CTAB-nano-BN after adsorption of dyes from the binary system

3.1.3 X-ray diffraction

The chemical examination of ca-bentonite, CTAB-nano-BN, and the sorbent after adsorption of dyes was performed using X-ray diffraction (XRD). The patterns of raw bentonite are shown in Figure 7(A), with respect to SiO_2 and Al_2O_3 being the major mineral constituents for each sample [40]. The XRD analysis of all samples shows that it is a calcium bentonite and is made up of several mineral phases; peaks at 29–32°, 39–42°, and 45–50° are associated with calcium-containing minerals such as CaO and calcium silicates, confirming that bentonite is rich in calcium [41]. The main peak at 2θ around 26.6° matches that of quartz (SiO_2), a major mineral in the sample [42]. The pattern shown in Figure 7(B) refers to CTAB-nano-BN, where the main crystalline phases of bentonite clay are observed at 2θ (21.46°, 35.401°, 50.93°, and 63.553°), which are attributed to the presence of the clay mineral SiO_2 [43, 44]. The peaks at 2θ (31.415°, 45.298°) are due to the presence of zinc oxide nanoparticles, which were also found by some studies [12, 39].

The main reason for the disappearance of most of the peaks belonging to CaO is the replacement of hydrated cations by quaternary ammonium cations returning to CTAB ions via ion exchange [26, 45].

The decrease in the intensity of some peaks in the diffraction of the sample CTAB-nano-BN is due to the incorporation of metal oxide nanoparticles into the clay and their dispersion on the bentonite surface [46-48].

Following adsorption of the two-MG and RR 152 dyes from the binary system, as shown in Figure 7(C), several changes in the X-ray pattern are observed. These include shifts of key peaks, such as the SiO_2 peak shifting from 21.34° to 27°, as well as the appearance of new peaks for the main clay components, such as SiO_2 and Al_2O_3. Zinc oxide nanoparticles may have dominated these peaks. After adsorption, the crystalline phase of the modified bentonite rearranged, releasing these peaks. We also observed that the phase intensity decreased after adsorption, indicating that the adsorbent surface was coated with the two dye molecules. MG and RR 152 are large organic dyes that penetrate the pores of the clay and the surface of the bentonite. Due to the abundance of oppositely charged dyes, both negatively and positively charged dyes are attracted to the active sites and cover most of

the peaks [49].

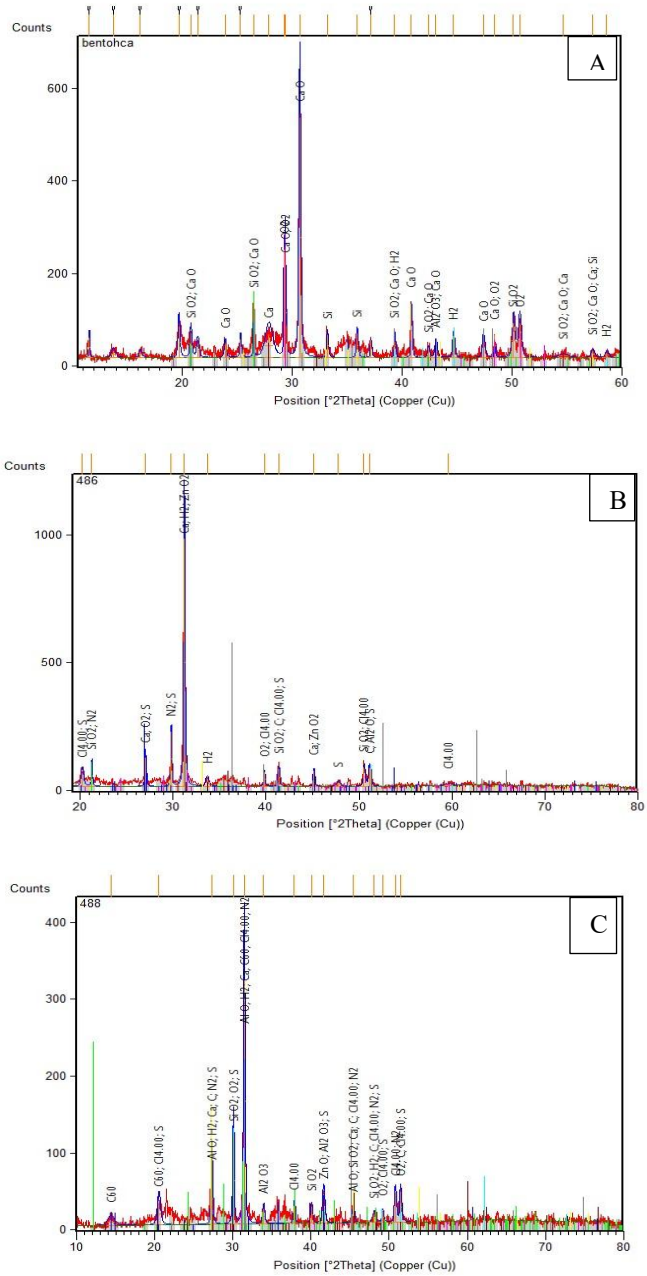

Figure 7. X-ray diffraction (XRD) analysis of (A) raw-bentonite, (B) CTAB-nano-BN, and (C) CTAB-nano-BN after adsorption of dyes from the binary system

3.1.4 Brunauer–Emmett–Teller analysis

Table 3 shows the Brunauer–Emmett–Teller (BET) surface areas and average pore diameters of raw BN and CTAB-nano-BN. BET analysis revealed that the specific surface area (S_{BET}) increased from 60.72 m²/g for raw BN to 157.48 m²/g for CTAB-nano-BN. The average pore diameter for raw BN and CTAB-nano-BN was 4.32 and 6.76 nm, respectively, indicating a mesoporous structure. The larger pore diameter of CTAB-nano-BN may provide more accessible pathways for the diffusion of dye molecules into the adsorbent. Furthermore, pore volume increased from 0.12 cm^3/g for raw BN to 0.29 cm^3/g for CTAB-nano-BN. The increase in surface area, average pore diameter and pore volume of CTAB-nano-BN likely results from CTAB modifying the layered structure. At the same time, ZnO nanoparticles provide additional surface area and maintain spacing between sheets [50].

Table 3. Textural characteristics of raw BN and CTAB-nano-BN

Samples	S_{BET} (m²/g)	Average Pore Diameter (nm)	Pore Volume (cm^3/g)
Raw BN	60.72	4.32	0.12
CTAB-nano-BN	157.48	6.76	0.29

3.2 Batch adsorption studies for malachite green and reactive red 152 dyes from a single system

As shown in Figures 8-11, the percentage of MG dye removal was high across various conditions, exceeding 99%. This is due to the strong electrostatic attraction between the adsorbent surface and the dye, and to the availability of sufficient active sites for adsorption. Largo et al. [51] used CTAB-modified magnetic sepiolite to remove MG dye and found that the maximum removal of 99.6% was obtained at a dose of 1 g, pH = 8, and 40 mg/L, with an equilibrium time of 240 min.

On the other hand, for the RR 152 dye, a high removal percentage of (99.23 ± 0.4)% was achieved at an adsorbent dose of 1 g and a concentration of 60 mg/L over the studied time period and at an acidic pH, as shown in Figure 11. El Mahbouby et al. [52] found that the maximum removal of Reactive Blue 19 does not exceed 90% at 0.6 g organo-clay (organo-ghassoul clay), at pH 5 and an initial concentration of 120 mg/L.

3.3 Batch adsorption studies for malachite green and reactive red 152 dye from binary system

3.3.1 Effect of CTAB-nano-BN dose on the removal rate of malachite green and reactive red 152 dyes

Figure 8 shows the effect of CTAB-nano-BN dose on the removal of MG and RR 152 dyes. It can be seen from Figure 8 that the removal rate of MG dye was more than 99% across all amounts of adsorbent at SD values ranging from 0.50 to 0.54. The stability of cationic dye removal stems from its high affinity for the sorbent, which has numerous active sites. Furthermore, the MG dye adsorption relies not only on electrostatic attraction with the clay but also on ion exchange with the anionic dye.

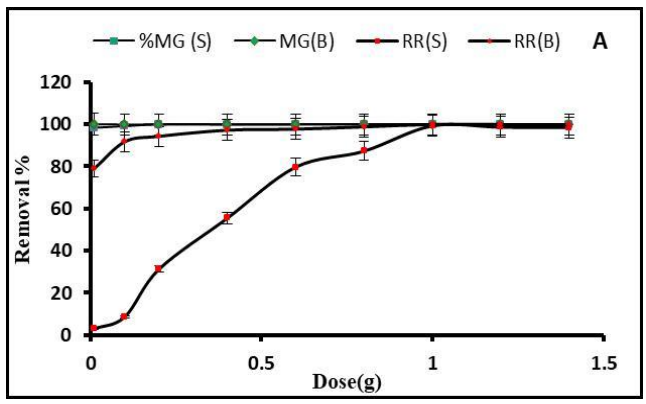

Figure 8. Influence of the amount of CTAB-nano-BN on the removal percentage of malachite green (MG) and reactive red 152 (RR 152) dyes from single (S) and binary (B) systems

In contrast, the removal rate of RR 152 dye increased from (78.8 ± 0.44)% to (99.9 ± 0.36)%. The gradual increase in removal rate is due to increasing sorbent dosage, which increases the number of active positive sites resulting from the organic modification. Arafa et al. [53] found that the sodium alginate-activated carbon/OMMT hydrogel (NaAlg/BLAC/OMMT) adsorbent was used for the removal of cationic MB dye and anionic EBT, with a maximum removal rate of 91.6% at a dose of 0.1 g for MB and 84% for EBT dye at 90 min.

3.3.2 The effect of initial concentration of malachite green and reactive red 152 dye

Figure 9 displays the impact of initial MG and RR 152 dye concentrations on the removal rate of MG and RR 152 dyes from non-competitive and competitive systems. Figure 9 shows a 99% removal rate for MG dye with a relatively low SD value and increases RR 152 dye removal from (75.6 ± 0.4)% to (99 ± 0.41)% across all studied concentrations, demonstrating that the prepared organic nano-BN is highly efficient. The complete removal of the dye across the studied concentrations indicates the high affinity of the dye for the nano-organic bentonite. The dye quickly occupies the active sites even at low concentrations. The low removal rate for the anionic dye is attributed to the limited number of available positive sites and the weak driving force of the dye molecules towards those sites. At higher concentrations, the driving force increases, leading to a higher removal rate.

Shirazi et al. [54] reported that the removal of RR195 and BV16 dyes from a binary system using vermicompost and Persian charred dolomite as adsorbents, when studying the impact of dye concentration within a range of 10 to 50, showed that the highest removal percentage was 85.6% for BV16 and 84% for RR195.

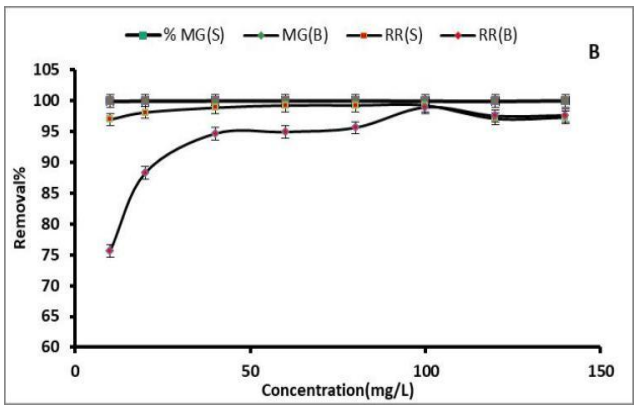

Figure 9. Influence of initial malachite green (MG) and reactive red 152 (RR 152) dye concentrations on the removal efficiency from single (S) and binary (B) systems

3.3.3 Effect of contact time on the removal efficiency

Results for the binary system which indicating 99.99% removal of MG dye across all studied adsorption times. As for the RR 152 dye, the removal rate was high, with removal exceeding 99% at contact periods with a low SD, as can be seen in Figure 10. In a binary system based on the adsorption of two dyes with opposite charges, the adsorption process proceeds as follows: Initially, due to the presence of cationic active groups introduced by the ZnO Nanocomposite in CTAB-nano-BN, the negatively charged RR 152 dye molecules are attracted to these groups via electrostatic forces. The negatively charged RR 152 dye contains additional negatively charged groups in its structure, which act as new adsorption sites to attract the positively charged MG dye. Li et al. [55] found that the removal of MG and Congo red using waste masks and lignin had a removal rate of less than 20% at the first contact time (10 min) until it reached maximum efficiency of 80% and 43% for MG and CR, respectively, at 180 min.

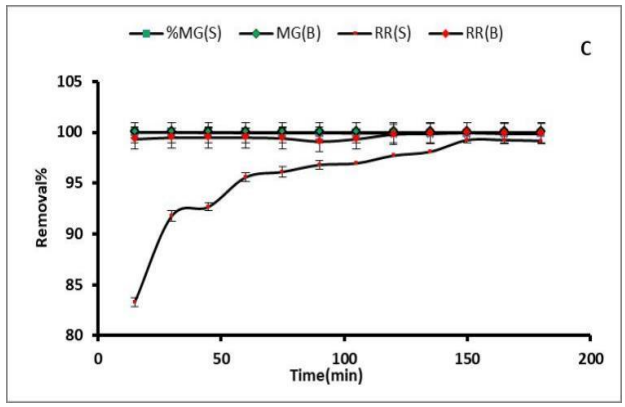

Figure 10. Effect of contact time on the dye removal efficiency from single (S) and binary (B) systems

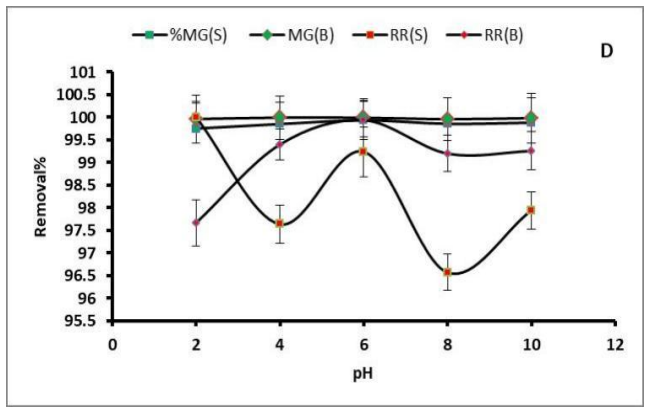

Figure 11. Effect of pH value on the removal efficiency of malachite green (MG) and reactive red 152 (RR 152) dyes from single (S) and binary (B) systems

3.3.4 Effect of PH value on removal efficiency

In order to study the effect of initial pH on the removal percentage of MG and RR 152 dyes onto CTAB-nano-BN, the batch balance study was executed in the pH range of 2–10, while other parameters remained constant. The initial dye concentrations in the binary system were fixed at 100 mg/L for MG and RR 152 dyes, the CTAB-nano-BN dose at 1 g/100ml, and the contact time at 120 min. The relation between the pH of the solution and the percentage removal of MG and RR 152 dyes is shown in Figure 11. For MG dye, the results are apparently unaffected by changes in pH value of the solution pH due to the dye's high affinity for the adsorbent and the availability of active sites. In contrast, RR 152 dye shows the opposite behavior in the single system. The removal rate increases with increasing pH value because of the availability of positive ions from the cationic dye addition to cationic active sites resulting from organic modification on CTAB-nano-BN. Lv et al. [56] found that yeast/cyclodextrin polymer composites removed MB and MO, with the highest removal occurring in alkaline and acidic media, respectively. Table 4

illustrates the comparison between the present study and this study.

The optimal operating conditions for the adsorption process were determined using the "one-factor-at-a-time" method; in each experiment, a single operating factor was varied while the others were held constant at previously established optimal values and the same variables were used for both single and binary systems. The optimal level for each factor was selected based on the highest removal efficiency achieved within the studied range, as shown in Tables 5 and 6.

Table 4. Comparison of CTAB-nano-BN in the removal of malachite green (MG) and reactive red 152 (RR 152) dyes with several reported adsorbents

Adsorbent	Adsorbate	Removal Rate	Optimum Condition	Refrences
MgO-impregnated clay	MG	97.04	Adsorbent dose 1 g, contact time 60 min, and concentration 50 mg/L	[57]
ZnO-bentonite clay	MG	98%	20 mg/L dye, 20 mg catalyst, 50 ℃, pH 6	[58]
MMTA and CTAB	Single system of Methyl orange Rhodamine B	98.7 98.4	At 100 mg/L(MO) 150 mg/L(RB), 0.5 g/L and pH 7	[59]
MMTA and CTAB	Xylenol orange	Maximum removal rate	Maximum removal at dose 0.12 g, 50 mg/L, 30 min, and pH 4	[60]
CTAB-modified Iraqi red kaolin	Methyl Blue	Maximum removal rate	Time 75 min, dose 0.1 g/100 mL, pH 4, and initial concentration 100 mg/L	[61]
BN/33% ZnO fabrication with HDTMA	Xylenol Orange	97%	Time 30 min	[50]
CTAB-nano-BN	Binary system of MG RR	99.9% (MG) 99.9% (RR)	All studied range for MG dye And for RR 152 dye (1 g CTAN-NANO-BN, 100 mg/L concentration, at time 60 min, and pH 6)	This study

Table 5. Listing the chosen optimum conditions for the single adsorption system for malachite green (MG) and reactive red 152 (RR 152) dyes

Parameters	Range Investigated	Constant Condition	Selected Optimum		Optimization Criterion	
			MG	RR 152	MG	RR 152
Adsorbent dose (g)	0.01–1.4	100 mg/L, 60 min, and pH 6	CTAB-nano-BN (0.01–1.4 g), concentration (10–100 mg/L), time (15–180 min), and pH (2–10)	1 g	99.9%	99.2%
Initial concentration (mg/L)	10–140	1 g dose, 60 min, and pH 6		100 mg/L	99.9%	99.2%
Time (min)	15–180	1 g dose, 100 mg/L, and pH 6		60 min	99.9%	96%
pH	2–10	1 g dose, 100 mg/L, and 60 min		6	99.9%	99.2%

Table 6. Listing the chosen optimum conditions for the binary adsorption system for malachite green (MG) and reactive red 152 (RR 152) dyes

Parameters	Range Investigated	Constant Condition	Selected Optimum		Optimization Criterion	
			MG	RR 152	MG	RR 152
Adsorbent dose (g)	0.01–1.4	100 mg/L for MG, 100 mg/L for RR, 60 min, and pH 6	CTAB-nano-BN (0.01–1.4 g), concentration (10–100 mg/L), time (15–180 min), and pH (2–10)	1 g	99.9%	99.9%
Initial concentration (mg/L)	10–140	1 g dose, 60 min, and pH 6		100 mg/L	99.9%	99.9%
Time (min)	15–180	1 g dose, 100 mg/L for MG, 100 mg/L for RR, and pH 6		60 min	99.9%	99.4%
pH	2–10	1 g dose, 100 mg/L for MG, 100 mg/L for RR, and 60 min		6	99.9%	99.9%

3.4 Adsorption isotherm for single and binary systems

The experimental data were fitted with various isotherm models to provide a theoretical basis for the operational design and the application of dye removal by adsorption. Langmuir and Freundlich models were used for the single system, and for the binary system, the Extended Langmuir (EL) isotherm, the Extended Freundlich (EF) isotherm, and the Jain and Snoeyink Modified Extended Langmuir (JSME) models were used to describe binary adsorption behavior, as shown in Table 7, where C_e is the equilibrium concentration (mg/L), $C_{e,1}$ and $C_{e,2}$ are for MG and RR 152 dyes, respectively; q_{max}: max.

adsorption capacity of the adsorbent (mg/g); $q_{max,1}$ and $q_{max,2}$ for dye 1 and dye 2 in a single system; k_b (L/mg) and k_l (L/g): Langmuir constants; k_f: Freundlich constant, and 1/n represents adsorption intensity.

Table 7. Models and equations of adsorption isotherms used for comparison

Model	Equation	References
Langmuir Equation (LE)	$\frac{C_e}{q_e} = \frac{1}{K_b q_{max}} + \frac{C_e}{q_{max}}$	[62]
Freundlich Equation (FE)	$\log(qe) = \log(kf) + \frac{1}{n}\log(Ce)$	[63]
Extended Langmuir (EL)	$qe,i = \frac{Q_{max,i}K_{L,i}C_{e,i}}{1+\sum_{j=1}^{N} K_{L,i}C_{e,i}}$	[64]
Extended Freundlich (EF)	$q_{e,i} = \frac{K_{f,i}C_{e,i}^{(n_i+x_i)}}{c_{e,i}^{x_i} + y_i c_{e,j}^{z_i}}$	[65]
Jain and Snoeyink Modified Extended Langmuir (JSME)	$q_{e,1} = \frac{(q_{max,1}-q_{max,2})k_{l,1}c_{e,1}}{1+k_{l,1}c_{e,1}} + \frac{q_{max,2}k_{l,1}c_{e,1}}{1+k_{l,1}c_{e,1}+k_{l,2}c_{e,2}}$ $q_{e,2} = \frac{q_{max,2}k_{l,2}c_{e,2}}{1+k_{l,1}c_{e,1}+k_{l,2}c_{e,2}}$	[66]

Parameters obtained from applying the linearized equations of the "Langmuir" and "Freundlich" models for the adsorption of MG and RR 152 dyes onto CTAB-nano-BN for single and binary systems are represented in Table 8. Based on the coefficient of determination value in the single system, the adsorption behavior of the two dyes exhibited distinct characteristics, reflecting different interaction mechanisms on the surface of CTAB-nano-BN due to the properties of the adsorbent surface. The RR 152 dye conformed better to the Langmuir model, indicating that the experimentally obtained adsorption data of RR 152 dye are more consistent with adsorption on a homogeneous surface with uniform energies. Al Rubai et al. [43] found the same result when studying the removal of RR120 using CTAB-BN. The MG dye, by contrast, conformed better to the Freundlich model, which shows that the experimental adsorption data for MG dye are more consistent with a heterogeneous adsorption surface and varying adsorption energies [57]. Despite the agreement of the experimental data with both models, this does not provide conclusive evidence regarding the mechanism of adsorption—whether it is monolayer or multilayer. Table 8 shows the decrease in the q_{max} value of the MG dye in the binary system, which indicates that the adsorption of its molecules is affected by the presence of the negative RR 152 dye, while the increase in the q_{max} value of the RR 152 dye in the competitive system indicates that the adsorption of this dye improves in the presence of the cationic MG dye. Furthermore, the fact that the Kl value of the cationic dye is greater than that of the negative dye in both the single and binary systems indicates the high affinity of the cationic dye for the adsorbent in both systems.

Table 8. Langmuir and Freundlich isotherm constants for malachite green (MG) and reactive red 152 (RR 152) dyes in single and binary systems

Model	Parameters	MG Dye		RR 152 Dye	
		Single System	Binary System	Single System	Binary System
	q_{max} (mg/g)	192.307	79.4	16	17.4
	Kb	1.21	5.99	0.24	2.73
Langmuir	Kl	232.5	476.19	3.84	47.62
	R^2	0.8389	0.6884	0.9873	0.9035
	RL	0.0082	0.0016	0.04	0.0036
	1/n	0.791	0.3826	0.2266	0.6925
Freundlich	kf	112.5	132.5	5.96	40.4
	R^2	0.9495	0.7848	0.9187	0.8826

Table 9. Equations of goodness-of-fit measures

Parameters	Equation	References
Sum of squared errors (SSE)	$SSE = \sum_{i=1}^{n}(qe.cal - qe.exp)^2$	[67]
Chi-square (χ^2)	$X^2 = \sum_{i=1}^{n}\frac{(qe.cal - qe.exp)^2}{qe.cal}$	[67]
Root mean square error (RMSE)	$RMSE = \sqrt{\frac{\sum_{i=1}^{n}(qe.cal - qe.exp)^2}{N}}$	[68]

The goodness-of-fit of the adsorption models was evaluated using the sum of squared errors (SSE), the root mean square error (RMSE), and the non-linear chi-square value (χ^2) and their equations in Table 9. Error functions were calculated from differences between experimental and model-calculated adsorption capacities; lower values of these parameters indicate less deviation between experimental and predicted capacities, indicating a better model fit.

From Figures 12 and Table 10, the theoretical value for MG dye adsorption in a binary system with RR 152 dye, using JSME, best matches the MG and RR 152 dyes, with the lowest SSE, X2, and RMSE values. This indicates that the presence of the co-existing dye influenced the equilibrium behavior of the two dyes in the binary system, and that the presence of one dye altered the adsorption behavior of the other; this may be attributed to the nature of the bentonite modified with CTAB and zinc oxide nanoparticles, which creates competition between the two dyes for adsorption sites of varying charges. Kılıç and Orhan [69] argued that the EL models failed to describe the balance data for removing two positive dyes from

a binary system. Othmani demonstrated that the elimination of cationic dyes from a binary system agrees with the JSME model [70].

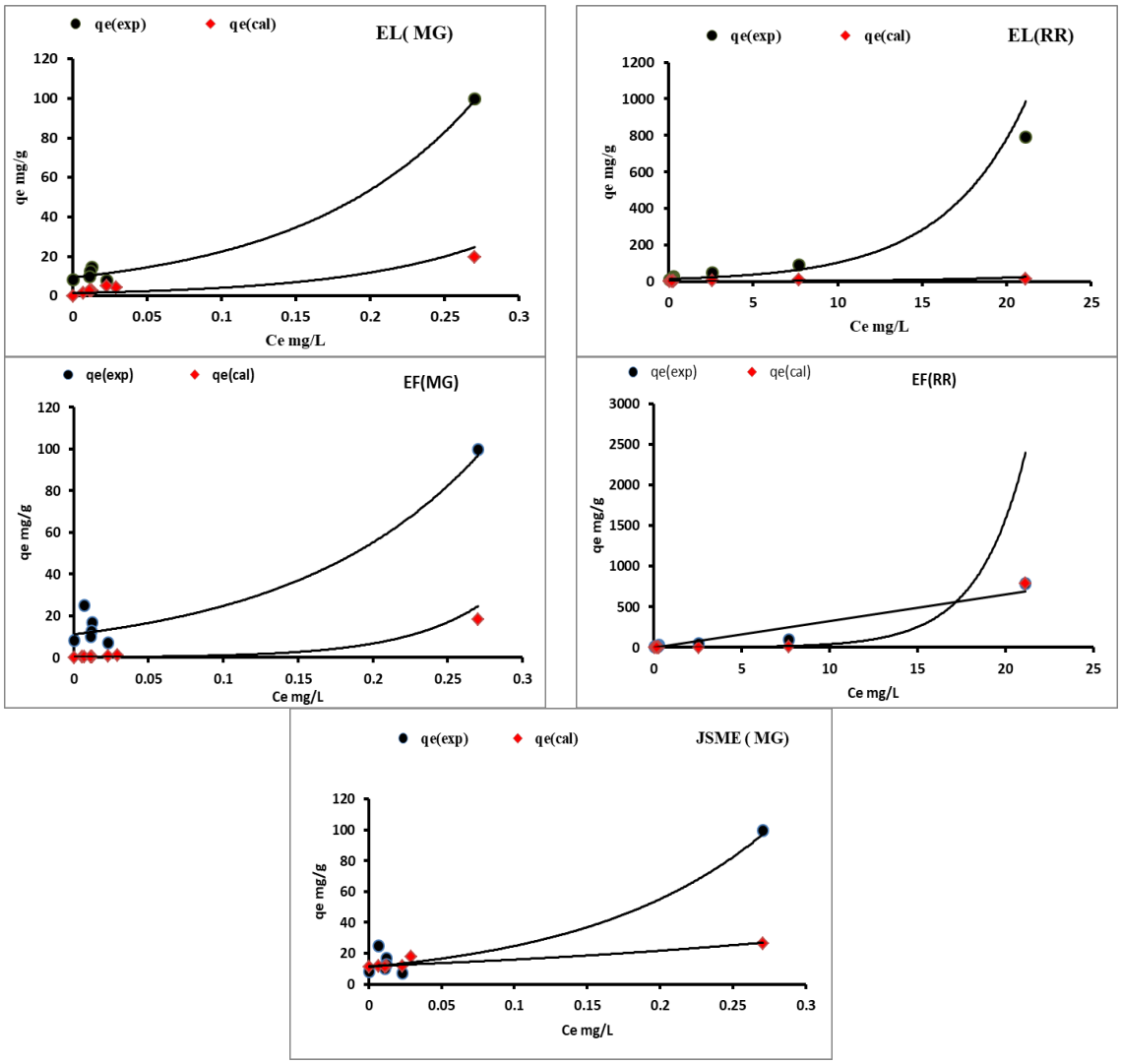

Figure 12. Isotherm models for malachite green (MG) dye in a binary system with reactive red 152 (RR 152) dye

Table 10. Sum of squared errors (SSE), chi-square (χ^2), and root mean square error (RMSE) values of malachite green (MG) and reactive red 152 (RR 152) dyes for isotherm models

Model	MG Dye			RR 152 Dye		
	SSE	X^2	RMSE	SSE	X^2	RMSE
EL	6809	1247	28	610726	47649	261
EF	7893.2	20329	30	10700	3.58E+10	34.5
JSME	5916	240	26	610726	47649	261

Note: MG = RMSE, RR = RMSE.

Table 11. The parameters of Kinetic models of malachite green (MG) and reactive red 152 (RR 152) dyes in single and binary systems

Kinetic Model	Parameters	Single System		Binary System	
		MG	RR	MG	RR
	R^2	0.8752	0.6422	0.8787	0.7075
PFO	$q_{e,cal}$ (mg/g)	0.9995	1.117	0.0037	0.0815
	$q_{e,exp}$ (mg/g)	9.99	9.8	9.999	9.985
	k_1 l/min	$6.9*10^{-6}$	$6.9*10^{-4}$	0.066	0.0165
PSO	R^2	1	0.9999	1	1
	qe, exp (mg/g)	9.99	9.8	9.9994	9.9852
	$q_{e,cal}$ (mg/g)	10	10.03	10	10
	k_2 l/min	11.133	0.0318	50	0.316

3.5 Kinetic study for single and binary dye system adsorption by CTAB-nano-BN

Studying kinetic models for dye adsorption in a binary system is important because it helps explain the reaction pathways and adsorption mechanisms. To analyze the experimental data for MG and RR 152 dyes in both single- and binary-dye systems, we used pseudo-first-order, pseudo-second-order, and interparticle diffusion models. We compared the results to see which model best described the adsorption process. We selected the most suitable model based on the linear correlation coefficient (R^2) and how closely the experimental and calculated maximum adsorption capacities ($q_{e,\,max,\,exp}$ and $q_{e,\,max,\,cal}$) matched for both dyes. According to the table, the pseudo-second-order kinetic model had the highest linear correlation coefficients for both dyes, with R^2 values of 1 for MG and RR 152. The experimental and calculated maximum adsorption capacities were also very close, as shown in Figure 13 and Table 11.

However, this agreement does not clearly indicate the adsorption mechanism specifically, whether it is chemisorption or governed by intra-particle diffusion. When applying the Weber–Morris model as illustrated in Figure 14, the plot does not pass through the origin; this implies that intra-particle diffusion was not the rate-controlling mechanism and that other mechanisms were involved. Consequently, we interpreted the kinetic results for adsorption of both dyes in both systems without precisely identifying the specific adsorption mechanism. These results are also consistent with the adsorption kinetics of the two dyes in the single system. These results are consistent with those obtained by Benamer-Oudih et al. [71], as the adsorption of methyl blue and methyl orange dyes by NPs is best fit by the second-order pseudo-kinetic model.

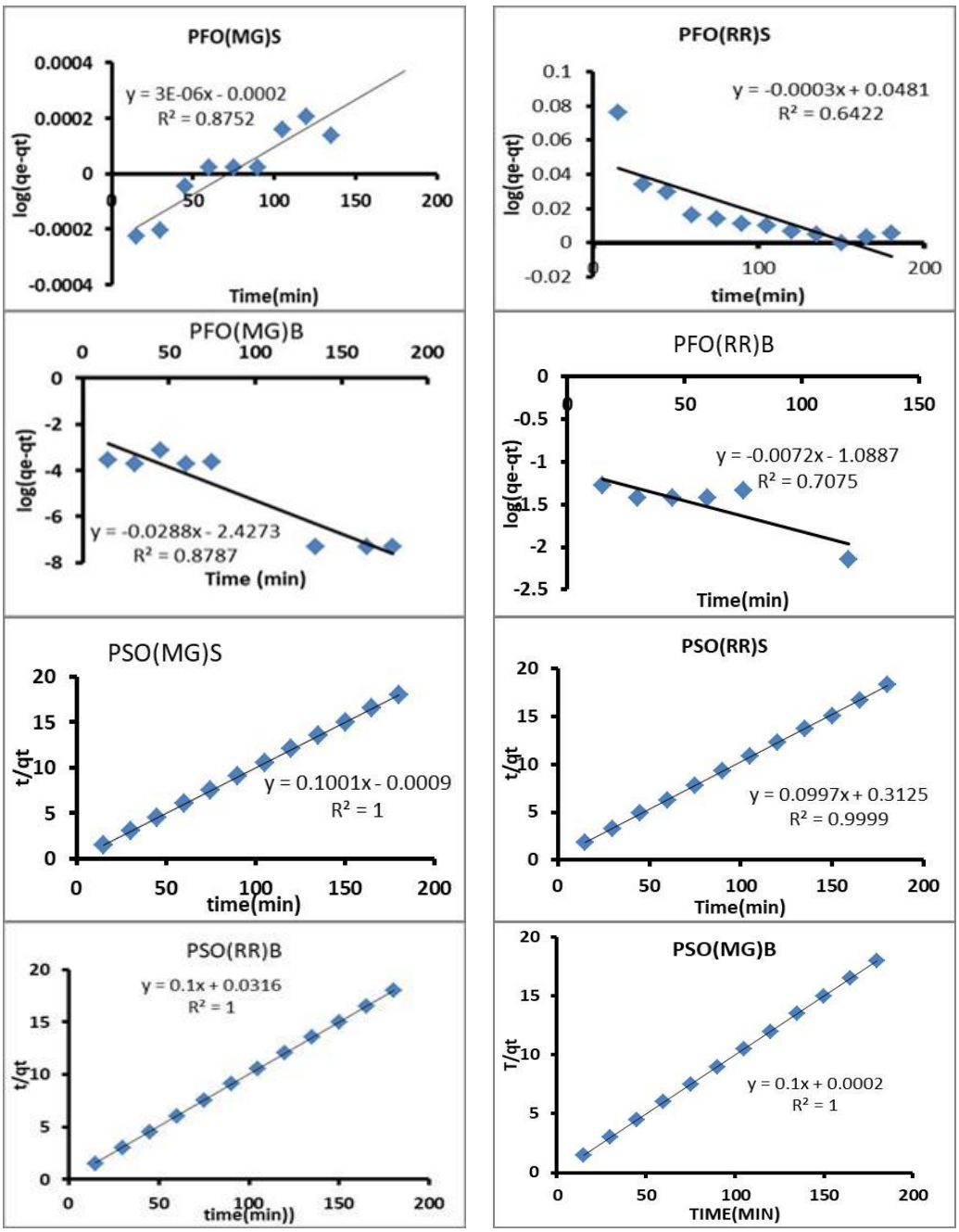

Figure 13. Kinetic models for malachite green (MG) and reactive red 152 (RR 152) dyes in single (S) and binary (B) systems

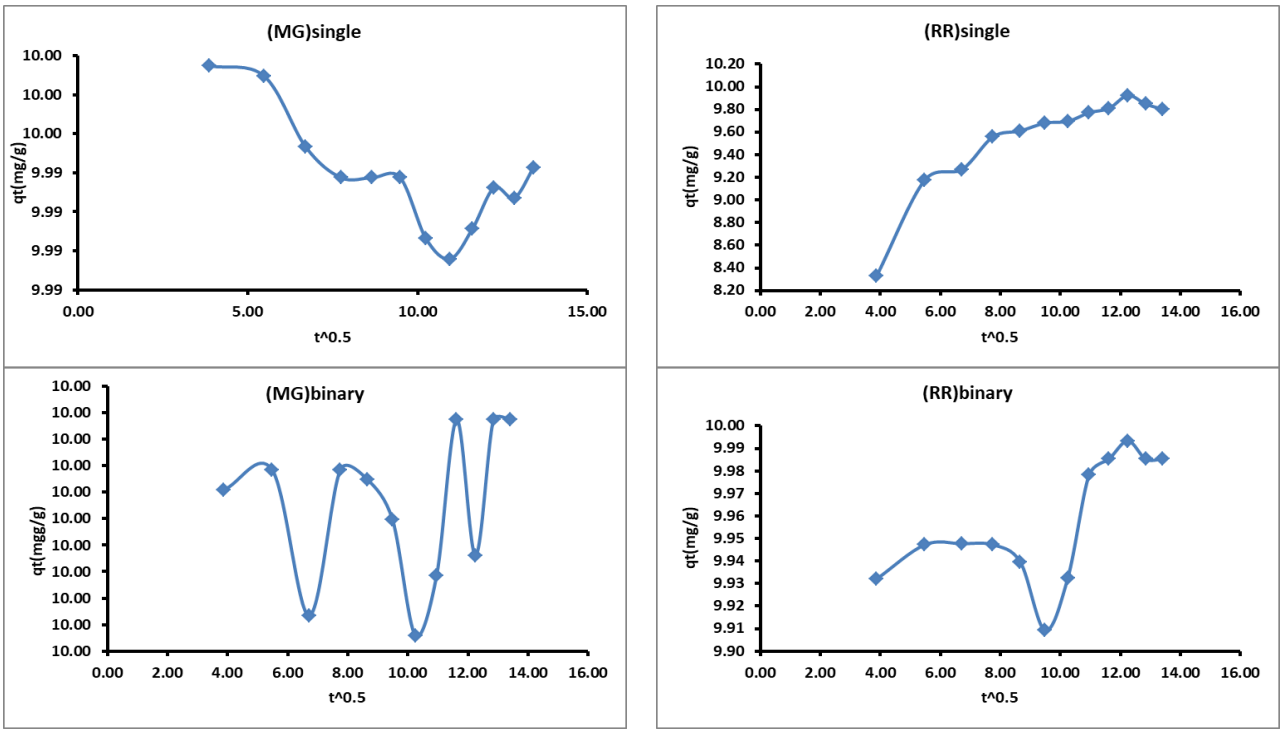

Figure 14. Weber–Morris model for malachite green (MG) and reactive red 152 (RR 152) dyes in single (S) and binary (B) systems

4. CONCLUSIONS

This study has shown that CTAB-nano-BN is an effective adsorbent for the adsorption of different charged dyes from aqueous solutions in mono- and competitive systems. The adsorbent showed high affinity for the MG dye with a removal rate of 99.99% under the different studied conditions, while maintaining a high removal rate for the RR 152 dye at a dose of 1 g, 100 mg/L, pH = 6, and 60 min, which were considered optimal operating conditions that achieved the highest removal efficiency. This highlights its ability to treat water containing dyes with different charges. Isotherm model analyses confirmed the suitability of the adsorption models. The kinetics model does not clearly indicate the adsorption mechanism. indicating the suitability of the effective adsorption behavior for the two dyes. Considering the high efficiency of CTAB-nano-BN under the conditions tested, availability, ease of preparation, and selectivity towards different dye systems.

REFERENCES

[1] Hanafi, M.F., Sapawe, N. (2020). A review on the water problem associate with organic pollutants derived from phenol, methyl orange, and remazol brilliant blue dyes. Materials Today: Proceedings, 31: A141-A150. https://doi.org/10.1016/j.matpr.2021.01.258

[2] Dutta, P., Rabbi, M., Sufian, M., Mahjebin, S. (2022). Effects of textile dyeing effluent on the environment and its treatment: A review. Engineering and Applied Science Letters, 5: 1-17. https://www.doi.org/10.30538/psrp-easl2022.0080

[3] Dutta, S., Adhikary, S., Bhattacharya, S., et al. (2024). Contamination of textile dyes in aquatic environment: Adverse impacts on aquatic ecosystem and human health, and its management using bioremediation. Journal of Environmental Management, 353: 120103. https://doi.org/10.1016/j.jenvman.2024.120103

[4] Mehra, S., Singh, M., Chadha, P. (2021). Adverse impact of textile dyes on the aquatic environment as well as on human beings. Toxicology International, 28(2): 165. https://doi.org/10.18311/ti/2021/v28i2/26798

[5] Cai, D., Zhang, Y., Li, J., et al. (2024). Intermolecular interactions in mixed dye systems and the effects on dye wastewater treatment processes. RSC Advances, 14(1): 373-381. https://doi.org/10.1039/d3ra01733h

[6] Rápó, E., Tonk, S. (2021). Factors affecting synthetic dye adsorption; desorption studies: A review of results from the last five years (2017–2021). Molecules, 26(17): 5419. https://doi.org/10.3390/molecules26175419

[7] Qi, J., Yu, J., Shah, K.J., Shah, D.D., You, Z. (2023). Applicability of clay/organic clay to environmental pollutants: Green way—An overview. Applied Sciences, 13(16): 9395. https://doi.org/10.3390/app13169395

[8] Islam, M.R., Mostafa, M.G. (2022). Adsorption kinetics, isotherms and thermodynamic studies of methyl blue in textile dye effluent on natural clay adsorbent. Sustainable Water Resources Management, 8(2): 52. https://doi.org/10.1007/s40899-022-00640-1

[9] Zhu, Y., Cui, Y., Peng, Y., Dai, R., Chen, H., Wang, Y. (2023). Preparation of CTAB intercalated bentonite for ultrafast adsorption of anionic dyes and mechanism study. Colloids and Surfaces A: Physicochemical and Engineering Aspects, 658: 130705. https://doi.org/10.1016/j.colsurfa.2022.130705

[10] Malsawmdawngzela, R., Lalhmunsiama, Tiwari, D. (2022). Novel and highly efficient functionalized bentonite for elimination of Cu2+ and Cd2+ from aqueous wastes. Environmental Engineering Research, 27(6): 210355. https://doi.org/10.4491/eer.2021.355

[11] Mahmoud, A.S. (2022). Effect of nano bentonite on

direct yellow 50 dye removal; adsorption isotherm, kinetic analysis, and thermodynamic behavior. Progress in Reaction Kinetics and Mechanism, 47: 14686783221090377. https://doi.org/10.1177/14686783221090377

[12] Jida, S.M., Zerefa, E.A. (2023). Preparation and photocatalysis of ZnO/bentonite based on adsorption and photocatalytic activity. Materials Research Express, 10(3): 035502. https://doi.org/10.1088/2053-1591/acbf0f

[13] Alshabanat, M., El-Saeid, M.H., Almuqati, N.S., et al. (2025). Preparation and characterization of ZnO/bentonite nanocomposites for enhanced photocatalytic degradation of pesticides in contaminated water. Scientific Reports, 15(1): 23816. https://doi.org/10.1038/s41598-025-09449-2

[14] Song, P.N., Mahy, J.G., Farcy, A., Calberg, C., Fagel, N., Lambert, S.D. (2024). Development of novel composite materials based on kaolinitic clay modified with ZnO for the elimination of azo dyes by adsorption in water. Results in Surfaces and Interfaces, 16: 100255. https://doi.org/10.1016/j.rsurfi.2024.100255

[15] Bentaleb, K., Bouberka, Z., Pierlot, C., Vandewalle, M., Volkringer, C., Maschke, U. (2023). Adsorption of orange G dye on hydrophobic activated bentonite from aqueous solution. Crystals, 13(2): 211. https://doi.org/10.3390/cryst13020211

[16] Khatibi, A.D., Yilmaz, M., Mahvi, A.H., Balarak, D., Salehi, S. (2022). Evaluation of surfactant-modified bentonite for Acid Red 88 dye adsorption in batch mode: Kinetic, equilibrium, and thermodynamic studies. Desalination and Water Treatment, 271: 48-57. https://doi.org/10.5004/dwt.2022.28812

[17] Mostafa, A.G., Abd El-Hamid, A.I., Akl, M.A. (2023). Surfactant-supported organoclay for removal of anionic food dyes in batch and column modes: Adsorption characteristics and mechanism study. Applied Water Science, 13(8): 163. https://doi.org/10.1007/s13201-023-01959-6

[18] Ardiyanti, A., Suprapto, S., Ni'mah, Y.L. (2023). Malachite green adsorption using carbon-based and non-conventional adsorbent made from biowaste and biomass: A review. Journal of Renewable Materials, 11(11): 3789-3806. https://doi.org/10.32604/jrm.2023.031354

[19] Mahida, V.P., Patel, M.P. (2016). A novel approach for the synthesis of hydrogel nanoparticles and a removal study of reactive dyes from industrial effluent. RSC Advances, 6(26): 21577-21589. https://doi.org/10.1039/c5ra19441e

[20] Iqajtaoune, A., Taibi, M.H., Saufi, H., Aouan, B., Boudad, L. (2024). Enhanced removal of methylene blue and procion deep red H-EXL dyes from aqueous environments by modified-bentonite: Isotherm, kinetic, and thermodynamic. Desalination and Water Treatment, 320: 100607. https://doi.org/10.1016/j.dwt.2024.100607

[21] Naji, A.M., Ali, Z.T.A. (2023). Evaluation of modified bentonite using chemical and physical methods for removal of amoxicillin from aqueous solutions: Batch and continuous study. Desalination and Water Treatment, 294: 185-201. https://doi.org/10.5004/dwt.2023.29564

[22] Al-Saade, K., Al-Safi, S., Al-Asadi, Z.A. (2013). Determination: The effect of ZnO on Iraqi bentonite surface properties. Baghdad Science Journal, 10(3): 49. https://doi.org/10.21123/bsj.2013.10.3.1034-1040

[23] Nasir, Z.A., Tlaiaa, Y.S., Ali, A.H. (2022). Design of dissolved air flotation (DAF) process for treating dyes-contaminated wastewater. Caspian Journal of Environmental Sciences, 20(2): 315-322. https://doi.org/10.22124/CJES.2022.5563

[24] Adeyi, A.A., Jamil, S.N.A.M., Abdullah, L.C., Choong, T.S.Y., Lau, K.L., Abdullah, M. (2019). Simultaneous adsorption of cationic dyes from binary solutions by thiourea-modified poly (acrylonitrile-co-acrylic acid): Detailed isotherm and kinetic studies. Materials, 12(18): 2903. https://doi.org/10.3390/ma12182903.

[25] Kgabi, D.P., Ambushe, A.A. (2023). Characterization of South African bentonite and kaolin clays. Sustainability, 15(17): 12679. https://doi.org/10.3390/su151712679

[26] Frida, E., Bukit, N., Bukit, F.R.A., Bukit, B.F. (2022). Analysis structure and morphology of bentonite-Opba nanocomposites as nanofillers. Journal of Applied Research and Technology, 20(2): 117-125. https://doi.org/10.22201/icat.24486736e.2022.20.2.1710

[27] Dolati, S., Kalani, M. (2021). Structural characterization of a bentonite deposit from the eastern Iran; Comparison with two reference bentonites. Carpathian Journal of Earth and Environmental Sciences, 16(1): 151-1rgo and others us. https://doi.org/10.26471/cjees/2021/016/163

[28] Olafadehan, O.A., Bello, V.E., Amoo, K.O. (2022). Production and characterization of composite nanoparticles derived from chitosan, CTAB and bentonite clay. Chemical Papers, 76(8): 5063-5086. https://doi.org/10.1007/s11696-022-02228-7

[29] Abukhadra, M.R., Saad, I., Othman, S.I., Allam, A.A., Fathallah, W. (2022). Synthesis of Co_3O_4@organo/polymeric bentonite structures as environmental photocatalysts and antibacterial agents for enhanced removal of methyl parathion and pathogenic bacteria. Journal of Inorganic and Organometallic Polymers and Materials, 32(7): 2600-2614. https://doi.org/10.1007/s10904-022-02346-5

[30] Agustian, E., Juwono, A.L., Rinaldi, N., Dwiatmoko, A.A. (2023). Pillaring of bentonite clay with Zr, Ti, and Ti/Zr by ultrasonic technique for biodiesel production. South African Journal of Chemical Engineering, 45(1): 228-239. https://doi.org/10.1016/j.sajce.2023.06.001

[31] Yang, C., Xu, H., Shi, J., Liu, Z., Zhao, L. (2021). Preparation and photocatalysis of CuO/bentonite based on adsorption and photocatalytic activity. Materials, 14(19): 5803. https://doi.org/10.3390/ma14195803

[32] Andrunik, M., Bajda, T. (2019). Modification of bentonite with cationic and nonionic surfactants: Structural and textural features. Materials, 12(22): 3772. https://doi.org/10.3390/ma12223772

[33] Hiranchansook, M., Jakpet, S., Trongsiriwat, N., Simasatitkul, L., Pranee, S., Seeyangnok, S. (2024). Enhancing oil absorption capacity through innovative bentonite modification with cationic surfactants. South African Journal of Chemistry, 78(1): 293-299. https://hdl.handle.net/10520/ejc-chem-v78-n1-a37.

[34] Ibrahim, S.M. (2020). Removal of acidic dye from aqueous solution using surfactant modified bentonite (organoclay): Batch and kinetic study. Journal of Engineering, 26(5): 64-81. https://doi.org/10.31026/j.eng.2020.05.05

[35] Wang, Y., Jiang, Q., Cheng, J., et al. (2021). Synthesis

and characterization of CTAB-modified bentonite composites for the removal of Cs^+. Journal of Radioanalytical and Nuclear Chemistry, 329(1): 451-461. https://doi.org/10.1007/s10967-021-07797-7

[36] My Linh, N.L., Duong, T., Van Duc, H., et al. (2020). Phenol red adsorption from aqueous solution on the modified bentonite. Journal of Chemistry, 2020(1): 1504805. https://doi.org/10.1155/2020/1504805

[37] Gaur, J., Kumar, S., Zineddine, M., et al. (2024). CTAB-crafted ZnO nanostructures for environmental remediation and pathogen control. Scientific Reports, 14(1): 20561. https://doi.org/10.1038/s41598-024-65783-x

[38] Al-Arjan, W.S. (2022). Zinc oxide nanoparticles and their application in adsorption of toxic dye from aqueous solution. Polymers, 14(15): 3086. https://doi.org/10.3390/polym14153086

[39] Abdel Salam, M., Abukhadra, M.R., Adlii, A. (2020). Insight into the adsorption and photocatalytic behaviors of an organo-bentonite/Co_3O_4 green nanocomposite for malachite green synthetic dye and Cr(VI) metal ions: Application and mechanisms. ACS Omega, 5(6): 2766-2778. https://doi.org/10.1021/acsomega.9b03411

[40] Fernandes, J.V., Rodrigues, A.M., Menezes, R.R., Neves, G.D.A. (2020). Adsorption of anionic dye on the acid-functionalized bentonite. Materials, 13(16): 3600. https://doi.org/10.3390/ma13163600

[41] Sultan, S., Karim, A., Permatasari, N.U. (2024). Green chemistry biosynthesis of calcium oxide nanoparticles as antibacterial waste microorganisms in waters. Ecological Engineering & Environmental Technology, 25(12): 233-252. https://doi.org/10.12912/27197050/194564

[42] Saad, I., Fathy, W.A., Amin, R.M., El-Dek, S.I. (2026). Physico-mechanical reinforcement and antimicrobial efficiency of green-synthesized Ca/bentonite/chitosan nanocomposites. Beni-Suef University Journal of Basic and Applied Sciences, 15(1): 8. https://doi.org/10.1186/s43088-025-00725-8

[43] Al Rubai, H.F., Hassan, A.K., Sultan, M.S., Abood, W.M. (2021). Kinetics of adsorption of Reactive Red 120 using bentonite modified by CTAB and study the effect of salts. Nature Environment and Pollution Technology, 20(1): 281-289. https://doi.org/10.46488/NEPT.2021.V20I01.031

[44] Nohong, N., Baratau, J.T.L., Wibowo, D., et al. (2025). Thermal activation and loading of clay/TiO2/CTAB composite: Physicochemical characterization and adsorption-photodegradation of methyl orange. Advances in Environmental Technology, 11(2): 193-206. https://doi.org/10.22104/aet.2025.6993.1920

[45] Parmar, S.P., Patel, B.S., Shukla, A., Dixit, M. (2022). Surfactant modified bentonite characterization: Effects and comparative analysis. Advances in Nanoscience and Nanotechnology, 7: 12-25.

[46] Akkari, M., Aranda, P., Rhaiem, H.B., Amara, A.B.H., Ruiz-Hitzky, E. (2016). ZnO/clay nanoarchitectures: Synthesis, characterization and evaluation as photocatalysts. Applied Clay Science, 131: 131-139. https://doi.org/10.1016/j.clay.2015.12.013

[47] Pamula, U.P., Rao, T.N., Prashanthi, Y., Ganji, P. (2025). Synthesis and characterization of ZnO@CTAB-SA polymer nanocomposites with biological and photocatalytic activity. Frontiers in Nanotechnology, 7: 1674700. https://doi.org/10.3389/fnano.2025.1674700

[48] Oukebdane, K., Necer, I.L., Didi, M.A. (2022). Binary comparative study adsorption of anionic and cationic azo-dyes on Fe3O4-bentonite magnetic nanocomposite: Kinetics, equilibrium, mechanism and thermodynamic study. Silicon, 14(15): 9555-9568. https://doi.org/10.1007/s12633-022-01710-x

[49] Ali, H., Ismail, A.M. (2023). Fabrication of magnetic Fe3O4/polypyrrole/carbon black nanocomposite for effective uptake of congo red and methylene blue dye: Adsorption investigation and mechanism. Journal of Polymers and the Environment, 31(3): 976-998. https://doi.org/10.1007/s10924-022-02663-3

[50] Obaid, A.A., Tameemi, H.M.A., Hameed, K.K. (2021). Fabrication of ZnO/nanobentonite as a new efficient adsorbent for rapid elimination of xylenol orange dye. Periodicals of Engineering and Natural Sciences, 9(1): 346-360. https://journals.ekb.eg/article_410263.html.

[51] Largo, F., Haounati, R., Ighnih, H., et al. (2024). Effective removal of toxic dye from wastewater via advanced modified magnetic sepiolite using combined surfactants SDS/CTAB/Fe3O4@Sep: Empirical and computational analysis studies. Journal of Molecular Liquids, 407: 125114. https://doi.org/10.1016/j.molliq.2024.125114

[52] El Mahbouby, A., Ezaier, Y., Zyade, S., Mechnou, I. (2023). Elaboration and characterization of organo-ghassoul (Moroccan clay) as an adsorbent using cationic surfactant for anionic dye adsorption. Physical Chemistry Research, 11(4): 913-928. https://doi.org/10.22036/pcr.2022.365510.2221.

[53] Arafa, E.G., Gawad, O.F.A., Eldin, Z.E., Ibrahim, M.M., Abd-Elghafour, S.A., Osman, A.H. (2025). Sustainable sodium alginate hydrogels incorporating banana leaf activated carbon and organo-clay for enhanced dye removal. Scientific Reports, 15(1): 16197. https://doi.org/10.1038/s41598-025-99343-8

[54] Shirazi, E.K., Metzger, J.W., Fischer, K., Hassani, A.H. (2019). Simultaneous removal of a cationic and an anionic textile dye from water by a mixed sorbent of vermicompost and Persian charred dolomite. Chemosphere, 234: 618-629. https://doi.org/10.1016/j.chemosphere.2019.05.224

[55] Li, P., Yang, C., Wang, Y., Su, W., Wei, Y., Wu, W. (2023). Adsorption studies on the removal of anionic and cationic dyes from aqueous solutions using discarded masks and lignin. Molecules, 28(8): 3349. https://doi.org/10.3390/molecules28083349

[56] Lv, Z., Wang, Z., Wang, H., Li, J., Li, K. (2024). Adsorption of cationic/anionic dyes and endocrine disruptors by yeast/cyclodextrin polymer composites. RSC Advances, 14(10): 6627-6641. https://doi.org/10.1039/d3ra07682b

[57] Moustafa, M.T. (2023). Preparation and characterization of low-cost adsorbents for the efficient removal of malachite green using response surface modeling and reusability studies. Scientific Reports, 13(1): 449. https://doi.org/10.1038/s41598-023-31391-4

[58] Gebrye, A.B., Mehari, B., Atlabachew, M. (2025). Photocatalytic performance of ZnO immobilized on bentonite for catalytic degradation of malachite green under sunlight irradiation. Hybrid Advances, 100542. https://doi.org/10.1016/j.hybadv.2025.100542

[59] Akl, M.A., El-Mahdy, N., Al-Awadhi, M.M., Mostafa, A. (2024). Cationic organo-montmorillonite for efficient

concomitant removal of anionic dyes in single and multi-components' solutions: Adsorption characteristics and mechanism study. Egyptian Journal of Chemistry, 67(1): 205-223. https://doi.org/10.21608/ejchem.2023.210347.7962

[60] Zheng, S., He, R., Fang, Z., et al. (2025). Optimized adsorption of xylenol orange dye in water systems employing CTAB-treated montmorillonite composite. Desalination and Water Treatment, 101595. https://doi.org/10.1016/j.dwt.2025.101595

[61] Saeed, B.M., Abdul-Kareem, M.B. (2025). Preparation and performance of a modified Iraqi red kaolin clay-based sorbent for methylene blue removal in acidic and basic solutions. International Journal of Design & Nature and Ecodynamics, 20(2): 241-249. https://doi.org/10.18280/ijdne.200203

[62] Saleh, Z.A., Hassan, A.A., Idan, I.J., Al-Isawi, R.H., Al Saleh, H.A.A. (2024). Peanut shell as a natural adsorbent for the removal of Acid Blue 25 from aqueous solution. Environmental Research, Engineering and Management, 80(1): 34614. https://doi.org/10.5755/j01.erem.80.1.34614

[63] Ebrahimzadeh, F., Akbari, A. (2025). Investigation the adsorption mechanisms, chemical resistance and mechanical strength of the synthesized chitosan/activated carbon composite in methylene blue removal. Scientific Reports, 15(1): 37820. https://doi.org/10.1038/s41598-025-21734-8

[64] Acharya, A., Jeppu, G., Girish, C.R., et al. (2024). Adsorption of arsenic and fluoride: Modeling of single and competitive adsorption systems. Heliyon, 10(11): e31967. https://doi.org/10.1016/j.heliyon.2024.e31967

[65] Danat, B.T., Wuana, R.A., Chahul, H.F., Iorungwa, M.S. (2026). Review of adsorption isotherms models. Applied Water Science, 16: 72. https://doi.org/10.1007/s13201-025-02682-0

[66] Amrutha, Jeppu, G., Girish, C.R., Prabhu, B., Mayer, K. (2023). Multi-component adsorption isotherms: Review and modeling studies. Environmental Processes, 10(2): 38. https://doi.org/10.1007/s40710-023-00631-0

[67] Eke-Emezie, N., Etuk, B.R., Akpan, O.P., Chinweoke, O.C. (2022). Cyanide removal from cassava wastewater onto H_3PO_4 activated periwinkle shell carbon. Applied Water Science, 12(7): 157. https://doi.org/10.1007/s13201-022-01679-3

[68] Ud Din, S., Al-Ahmary, K.M., AlMohamadi, H., et al. (2025). Low-cost and sustainable bioadsorbent from banana peel waste for crystal violet dye removal. BioResources, 20(4): 10640-10664. https://doi.org/10.15376/biores.20.4.10640-10664

[69] Kılıç, A., Orhan, R. (2019). Removal of cationic dyes by adsorption in a single and binary system using activated carbon prepared from the binary mixture. Separation Science and Technology, 54(14): 2147-2163. https://doi.org/10.1080/01496395.2019.1636068

[70] Othmani, A., Selatnia, A., Bachari, K. (2025). Sustainable biosorption of cationic textile dyes (BY28, BB41, BR46) from aqueous solutions using pharmaceutical waste biomass (Streptomyces rimosus): Comparative study in single, binary, and ternary systems. Journal of Water Process Engineering, 76: 108103. https://doi.org/10.1016/j.jwpe.2025.108103

[71] Benamer-Oudih, S., Tahtat, D., Nacer Khodja, A., et al. (2024). Sorption behavior of chitosan nanoparticles for single and binary removal of cationic and anionic dyes from aqueous solution. Environmental Science and Pollution Research, 31(28): 39976-39993. https://doi.org/10.1007/s11356-023-27907-0